Dalton Transactions

Light-induced electron transfer/phase migration of a redox mediator for photocatalytic C–C coupling in a biphasic solution

Journal:	*Dalton Transactions*
Manuscript ID	DT-ART-04-2022-001334.R1
Article Type:	Paper
Date Submitted by the Author:	19-May-2022
Complete List of Authors:	Itagaki, Ren; Chuo University Faculty of Science and Engineering Graduate School of Science and Engineering, Department of Chemistry Takizawa, Shin-ya; University of Tokyo, Chemistry Chang, Ho-Chol; Chuo University, Department of Applied Chemistry, Faculty of Science & Engineering Nakada, Akinobu; Chuo University Faculty of Science and Engineering Graduate School of Science and Engineering, Department of Chemistry

ARTICLE

Light-induced electron transfer/phase migration of a redox mediator for photocatalytic C–C coupling in a biphasic solution

Received 00th January 20xx,
Accepted 00th January 20xx

DOI: 10.1039/x0xx00000x

Ren Itagaki,[a] Shin-ya Takizawa,[b] Ho-Chol Chang,*[a] and Akinobu Nakada,*[a,c]

Photocatalytic molecular conversions that lead to value-added chemicals are of considerable interest. To achieve highly efficient photocatalytic reactions, it is equally important as it is challenging to construct systems that enable effective charge separation. Here, we demonstrate that the rational construction of a biphasic solution system with a ferrocenium/ferrocene (Fc^+/Fc) redox couple enables efficient photocatalysis by spatial charge separation using the liquid-liquid interface. In a single-phase system, exposure of a 1,2-dichloroethane (DCE) solution containing a Ru(II)- or Ir(III)-based photosensitizer, Fc, and benzyl bromide (Bn-Br) to visible-light irradiation failed to generate any product. However, the photolysis in a H_2O/DCE biphasic solution, where the compounds are initially distributed in the DCE phase, facilitated the reductive coupling of Bn-Br to dibenzyl (Bn_2) using Fc as an electron donor. The key result of this study is that Fc^+, generated by photooxidation of Fc in the DCE phase, migrates to the aqueous phase due to the drastic change in its partition coefficient compared to that of Fc. This liquid-liquid phase migration of the mediator is essential for facilitating the reduction of Bn-Br in the DCE phase as it suppresses backward charge recombination. The co-existence of anions can further modify the driving force of phase migration of Fc^+ depending on their hydrophilicity; the best photocatalytic activity was obtained with a turnover frequency of 79.5 h^{-1} and a quantum efficiency of 0.2% for the formation of Bn_2 by adding $NBu_4^+Br^-$ to the biphasic solution. This study showcases a potential approach for rectifying electron transfer with suppressed charge recombination to achieve efficient photocatalysis.

Introduction

Natural photosynthesis facilitates molecular-conversion reactions by capturing and transporting solar energy, charge migration, and catalysis in the reaction center.[1] Artificial photosynthetic reactions that mimic the natural system have been studied actively so far.[2-6] At the same time, photoredox catalysis has had great impact on the field of photochemical organic synthesis.[7, 8] In any case, photoinduced electron transfer from/to the electron donor(s)/acceptor(s) is a key initial step in these reactions.

One of the most important issues in the construction of artificial photocatalytic systems is to suppress undesired photoinduced electron transfer.[9-13] Taking reductive photocatalysis as an example, once a photosensitizer accepts an electron from a reductant upon photoexcitation, subsequent electron transfer to the catalytic site or substrate completes the targeted reaction (black arrows in Scheme 1a). On the other hand, backward charge recombination (red arrow in Scheme 1a) frequently diminishes the photocatalytic efficiency. For example, Ishitani and co-workers have reported that rapid backward charge recombination drastically decreases the photocatalytic quantum efficiency for the reduction of CO_2 using photocatalysts based on metal complexes.[4, 14, 15] Moreover, it has been reported that the backward charge recombination *via* reversible redox mediators such as IO_3^-/I^- or Fe^{3+}/Fe^{2+} deactivates the reduction and oxidation by semiconductor photocatalysts.[16-18] As shown in Scheme 1a, backward charge recombination after light-induced charge separation can always proceed considering the driving force. Therefore, it is strongly desirable to introduce a means into such systems that suppresses the undesirable backward charge recombination in order to improve the efficiency of various kinds of photocatalytic reactions.

Looking at natural photosynthesis, the photosystem assembly carries out multistep electron- and proton-transport processes crossing the interface of the Thylakoid membrane for an extremely efficient photogenerated charge transport, which results in an extremely high yield of light-to-chemical energy conversion.[19-23] Such phase migration phenomena also play important roles in synthetic chemistry,[24] analytical chemistry,[25] environmental science,[26, 27] electrochemistry,[28, 29] and catalysis.[7, 30]

[a] *Department of Applied Chemistry, Faculty of Science and Engineering, Chuo University, 1-13-27 Kasuga, Bunkyo-ku, Tokyo 112-8551, Japan.*
[b] *Department of Basic Science, Graduate School of Arts and Sciences, The University of Tokyo, 3-8-1 Komaba, Meguro-ku, Tokyo 153-8902, Japan.*
[c] *Precursory Research for Embryonic Science and Technology (PRESTO), Japan Science and Technology Agency (JST), 4-1-8 Honcho, Kawaguchi, Saitama 332-0012, Japan.*

† Electronic Supplementary Information (ESI) available. Cyclic voltammograms, emission spectra, UV-vis absorption spectra, decay curves of emission intensities, HPLC chromatograms, Photocatalytic activities of Bn-Br reduction, ^{1}H NMR spectra, emission dispersion X-ray spectra (PDF). See DOI: 10.1039/x0xx00000x

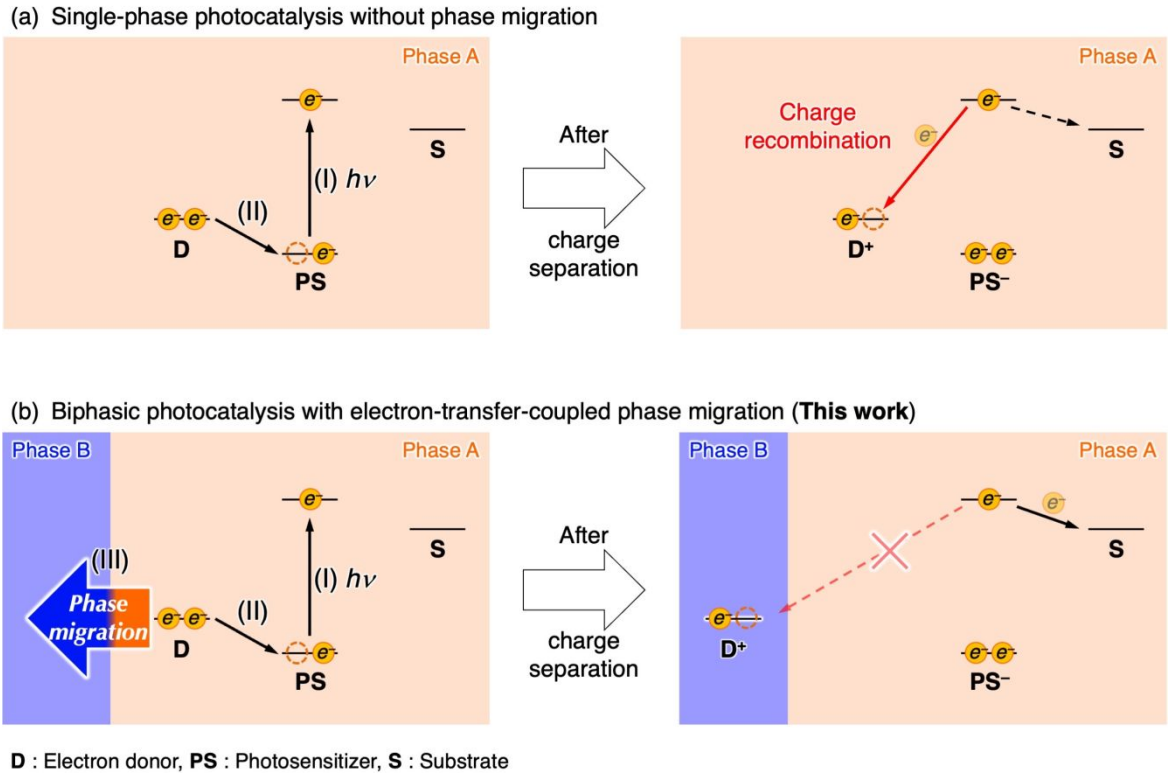

Scheme 1 Photoinduced electron transfer and backward charge recombination (a) without and (b) with coupled phase migration

Liquid-liquid phase migration triggered by electron transfer has been studied by electrochemical techniques at the three-phase interface of the electrode-liquid-liquid boundary.[31-33] A distinctly different solubility between oxidized and reduced species between two immiscible solvents is required for redox-directed phase migration because the changes in their distribution coefficient can serve as the driving force of phase migration. In this context, ferrocene (Fc) has been recognized as a suitable research target because it exhibits drastic solubility changes upon valence switching from neutral Fc to cationic ferrocenium (Fc^+).[34-36] For instance, White and co-workers have reported that electrochemical oxidation of Fc, unevenly distributed in the 1,2-dichloroethane (DCE) phase at the Pt-Ir/H_2O/DCE three-phase boundary, results in the migration of the generated Fc^+ in the DCE phase into the aqueous phase across the liquid-liquid interface.[37]

The redox-directed phase migration, which enables spatial separation of electron donor and acceptor between two immiscible solution phases, can be used as a rational tool to suppress the backward charge recombination in photocatalysis. Hence, we aimed to construct a phase-migration system driven by photoinduced electron transfer in a two-immiscible-solvent system as depicted in Scheme 1b; once a photosensitizer is excited by photoirradiation (Process I), the oxidized form of the electron donor, generated by the photoinduced electron transfer to a photosensitizer in one liquid phase A (Process II), migrates to another liquid phase B (Process III). This is expected to suppress the charge recombination due to the spatial separation between phase A and phase B. Peljo *et al.* reported that a similar concept is possible to construct the photo-ionic cells but never demonstrated.[38] Although biphasic solutions have been adapted to other photocatalysis, most of them do not involve phase migration of electron donor(s)/acceptor(s).[39, 40] Very recently, Nam and Fukuzumi have for the first time achieved overall water splitting into H_2 and O_2 using only a molecular photocatalytic system, by combination of a biphasic solution and a glass membrane.[41] Although this pioneering work implicates high utility of such biphasic solution systems in photocatalysis, the impact of phase migration of the electron mediator on the charge-separation/-recombination processes and photocatalytic efficiency have not yet been examined systematically. Herein, we investigate the photoinduced phase migration of Fc using $[Ru(dmb)_3](PF_6)_2$ (**Ru**; dmb = 4,4'-dimethyl-2,2'-bipyridine) and $[Ir(C6)_2(dmb)]PF_6$ (**Ir**; C6 = coumarin 6) as photosensitizers (Chart 1) in H_2O/DCE biphasic solution and its impact on the suppression of the backward charge recombination in the photochemical reduction of benzyl bromide (Bn-Br) as a benchmark reaction.[42-44] Moreover, we formulate design principles for accelerating the photoinduced phase migration in such biphasic photocatalytic systems.

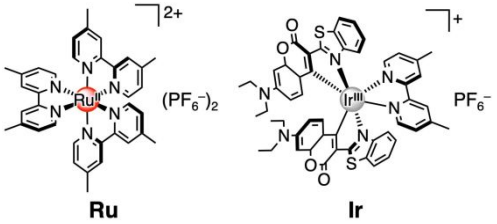

Chart 1 Structures and abbreviations of the Ru(II) and Ir(III) photosensitizers

Results and discussion

Electrochemical and photophysical properties of Fc, Bn-Br, and the Ru(II) and Ir(III) photosensitizers in 1,2-dichloroethane

The redox behavior of the photosensitizers and Fc was evaluated by electrochemical measurements (Fig. 1). Fc showed a quasi-reversible wave assigned to a metal-centered $Fe^{3+/2+}$ redox process at $E_{1/2}$ = 0.20 V vs. $Ag/AgNO_3$. In DCE, both **Ru** and **Ir** exhibited quasi-reversible waves corresponding to the first reduction process of the dmb ligand at $E_{1/2}$ = –1.65 and –1.53 V during the negative sweep and the metal-centered oxidation at $E_{1/2}$ = 0.98 and 0.93 V during the positive sweep, respectively (Fig. 1). The reduction and oxidation potentials of the excited photosensitizers (E^*_{red} and E^*_{ox}, respectively) were estimated by using the redox potentials of the ground state and previously-reported 0-0 excitation energies ($E_{0\text{-}0}$; 2.15 eV for **Ru** and **Ir**),[45, 46] on the basis of Eq. 1. The obtained redox potentials are listed in Table 1.

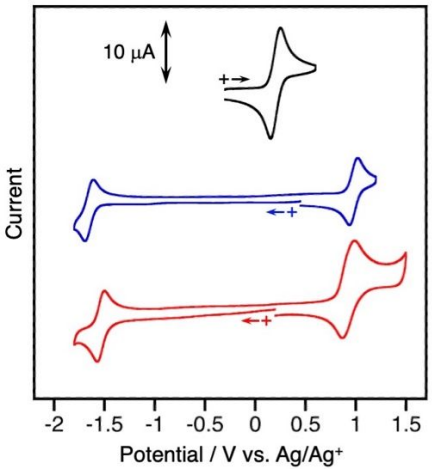

Fig. 1 Cyclic voltammograms of Fc (black), **Ru** (blue), and **Ir** (red) (0.5 mM) in DCE with $NBu_4^+PF_6^-$ (0.1 M) as the supporting electrolyte; scan rate: 0.1 V s^{-1}; working electrode: glassy carbon; reference electrode: $Ag/AgNO_3$ (0.01 M); counter electrode: Pt wire.

$$E^*_{red} = E_{red} + E_{0\text{-}0} \quad (1a)$$

$$E^*_{ox} = E_{ox} - E_{0\text{-}0} \quad (1b)$$

The E^*_{red} of **Ru** and **Ir** is ~300 mV more positively shifted relative to the E_{ox} of Fc (0.20 V), indicating that the reduction of excited photosensitizers by Fc is thermodynamically possible. The onset potential (E_{onset}) of the reduction of Bn-Br was found at approximately –1.5 V (Fig. S1). Therefore, the one-electron-reduced species of the photosensitizers, *i.e.*, $\mathbf{Ru}^-$ (E_{red} = –1.65 V) or $\mathbf{Ir}^-$ (E_{red} = –1.53 V) can be expected to reduce Bn-Br, while the excited states of the photosensitizers, *i.e.*, $\mathbf{Ru}^*$ (E^*_{ox} = –1.17 V) or $\mathbf{Ir}^*$ (E^*_{ox} = –1.22 V) cannot. In fact, the emission intensities of **Ru** or **Ir** in DCE did not change in the presence of Bn-Br, indicating that the electron transfer from the excited state of the photosensitizer to Bn-Br, *i.e.*, oxidative quenching, does not proceed (Fig. S2). Thus, electron relay from Fc to the excited states of photosensitizers is essential as the initial step during the photochemical reduction of Bn-Br (Processes I and II in Scheme 1).

The UV-vis absorption spectra of **Ru** and **Ir** in DCE show visible-light absorptions at maximum wavelengths of 460 and 482 nm, respectively (Fig. 2a). The former was assigned to the singlet metal-to-ligand charge transfer (^{1}MLCT),[47] whereas the latter was ascribed to the singlet ligand-centered (^{1}LC) electron transition of a minor contribution of the dmb ligand,[46] leading to an intense absorption of **Ir** (ε = 119,000 M^{-1} cm^{-1} at 482 nm), which is *ca.* eight times higher than that of **Ru** (ε = 15,000 M^{-1} cm^{-1}) Fc also showed an absorption band at 441 nm, albeit with a very low intensity (ε = 88 M^{-1} cm^{-1}) owing to its *d-d* nature (Fig. S3a). Conversely, Bn-Br does not absorb visible light (Fig. S3a), *i.e.*, it should be possible to excite **Ru** and **Ir** selectively using visible light. **Ru** and **Ir** exhibit phosphorescence at 630 nm (**Ru**) as well as 590 and 630 nm (**Ir**) with vibronic structures (Fig. 2a). The former was assigned to the phosphorescence of the triplet MLCT (^{3}MLCT) state,[48] while the latter was ascribed to the phosphorescence of the triplet LC (^{3}LC) of the coumarin-6 ligand center.[46] The lifetimes of the emissions are 0.7 and 25.6 μs for **Ru** and **Ir**, respectively (Fig. S4 and Table 1). The longer lifetime of **Ir** is due to phosphorescence from the ^{3}LC state.[46]

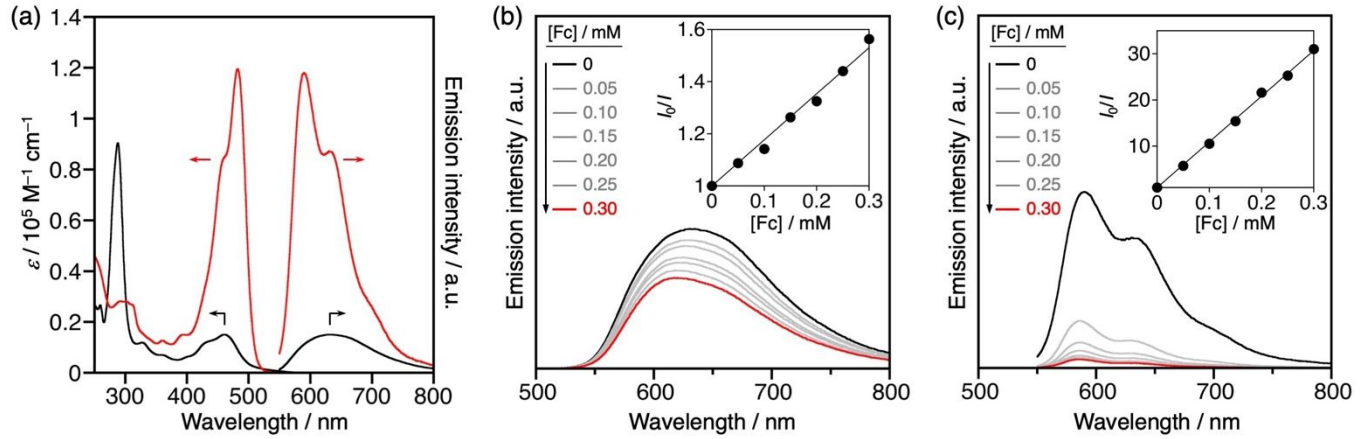

Fig. 2 (a) UV-vis absorption and emission spectra of **Ru** (black) and **Ir** (red) in DCE. (b,c) Emission spectra of **Ru** (b) and **Ir** (c) in the presence of Fc (0–0.3 mM) in DCE. The excitation wavelengths were 460 nm and 480 nm for **Ru** and **Ir**, respectively.

Table 1 Electrochemical and photophysical properties of **Ru** and **Ir** in DCE

photosensitizer	$E_{1/2}$ / V vs. $Ag/AgNO_3$ (ΔE_p / mV)		λ_{abs} / nm (ε_{max} / 10^3 M^{-1} cm^{-1})		λ_{em} / nm	τ_{em} / μs	k_q / 10^9 M^{-1} s^{-1}	η_q[a]
Ru	+0.98 (79)	–1.65 (82)	288 (88.5)	460 (14.7)	630	0.7	2.4	0.90
Ir	+0.93 (120)	–1.53 (75)	303 (27.9)	480 (119)	590	25.6	4.2	>0.99

[a]Quenching efficiency: $\eta_q = 1–\{1/(1 + k_q \tau_{em}[Fc])\}$ for [Fc] = 5.0 mM.

The photoinduced electron transfer was evaluated by means of emission-quenching measurements. Upon addition of Fc to the DCE solution containing **Ru** or **Ir**, the emission intensity of the photosensitizers decreased (Fig. 2b and c). It should also be noted here that Fc is not emissive (Fig. S3b), and thus does not directly affect the emission spectra. Considering the relationship between the redox potentials discussed above, the decreased emission was attributed to reductive quenching, *i.e.*, the reduction of the excited photosensitizer by Fc. The emission quenching follows Eq. 2a, where I and I_0 are the emission intensity in the presence and absence of Fc, respectively, K_{SV} is the Stern-Volmer constant, and [Fc] is the concentration of ferrocene, giving K_{SV} values of 1.8×10^3 and 1.1×10^5 M^{-1} for **Ru** and **Ir**, respectively.

$$I_0/I = K_{SV}[Fc] + 1 \quad (2a)$$

$$K_{SV} = k_q \tau_{em} \quad (2b)$$

Eq. 2b, where k_q denotes the quenching rate constant and τ_{em} the lifetime of emission, furnished quenching rate constants k_q of 2.4×10^9 M^{-1} s^{-1} (**Ru**) and 4.2×10^9 M^{-1} s^{-1} (**Ir**) in DCE. The similarity of the k_q values to the diffusion-limited rate constant k_{diff} (8×10^9 M^{-1} s^{-1} in DCE on the basis of the Debye relationship[49]) most likely suggests that the photoinduced electron transfer is a diffusion-controlled process for **Ru** and **Ir**. Therefore, the *ca.* sixty times higher K_{SV} of **Ir** compared to that of **Ru**, which can be expected to be beneficial for the efficiency of the photocatalysis, should most likely be attributed to its long-lived excited state (τ_{em} = 25.6 μs; Table 1 and Fig. S4b).

Photochemically induced reductive dimerization of Bn-Br using Fc as a phase-migratable electron donor

Considering the successful photoinduced electron transfer, it seems also feasible to expect that the photochemical reductive coupling of Bn-Br will be promoted by **Ru** or **Ir** when using Fc as the electron donor. Therefore, a DCE solution (1.5 mL) containing Fc (5.0 mM), **Ru** (0.5 mM), and Bn-Br (50 mM) under a nitrogen atmosphere was stirred and exposed to visible-light (λ > 400 nm) for 1 h (Entry 1, Table 2). However, the absorption spectrum remained unchanged (Fig. 3a), and dibenzyl (Bn_2) as the product of the Bn-Br reduction was not detected after photoirradiation (Fig. S5a and b). Given the redox reversibility of Fc (Fig. 1), the backward charge recombination can easily proceed from one-electron-reduced species of **Ru**, *i.e.*, $\mathbf{Ru}^-$ ($E_{1/2}$ = –1.65 V) to Fc^+ ($E_{1/2}$ = 0.20 V), which is thermodinamically much more favorable than the reduction of Bn-Br (E_{onset} ~ –1.5 V); accordingly, $\mathbf{Ru}^-$ and Fc^+ can return to the ground state, *i.e.*, **Ru** and Fc, without reducing Bn-Br (Scheme 1a, right).

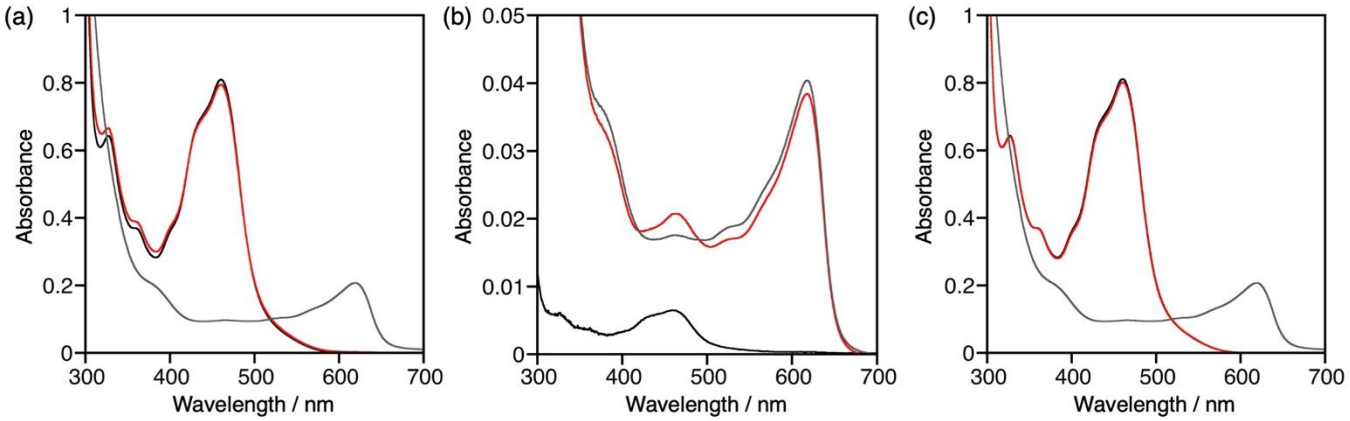

Fig. 3 UV-vis absorption spectra of (a) single-phase DCE solutions, and (b) aqueous and (c) organic phases in a H_2O/DCE biphasic solution containing **Ru** (0.5 mM), Fc (5 mM), and Bn-Br (50 mM) before (black) and after (red) irradiation with visible light (λ > 400 nm) for 1 h. The absorption spectrum of $Fc^+PF_6^-$ is shown as a reference (gray).

Table 2 Photochemical formation of Bn_2 and Fc^+ under varying conditions[a]

Entry	Component				Solution	Product	
	Photosensitizer	[Photosensitizer] / mM	[Fc] / mM	[Bn-Br] / mM		Fc^+ / μmol (TON)	Bn_2 / μmol (TON)
1	**Ru**	0.5	5.0	50	DCE	N.D.[b]	N.D.
2		0.5	5.0	50	H_2O/DCE	1.87 (2.49)	0.90 (1.20)
3[c]		0.5	5.0	50	H_2O/DCE	N.D.	N.D.
4		-	5.0	50	H_2O/DCE	N.D.	N.D.
5		0.5	-	50	H_2O/DCE	N.D.	N.D.
6		0.5	5.0	-	H_2O/DCE	0.12 (0.24)	N.D.
7		0.05	5.0	50	H_2O/DCE	0.14 (1.82)	N.D.
8	**Ir**	0.5	5.0	50	H_2O/DCE	1.90 (2.54)	1.42 (1.89)
9		0.05	5.0	50	H_2O/DCE	1.61 (21.5)	0.95 (12.7)
10		0.05	5.0	50	DCE	N.D.	N.D.
11[d]		0.05	5.0	50	H_2O/DCE	0.08 (1.10)	N.D.

[a]Visible light (λ > 400 nm) was used to irradiate the stirred sample solution for 1 h under a nitrogen atmosphere. [b]N.D. = Not detected. [c]In the dark. [d]Without stirring.

Interestingly, a very different result was obtained upon adding water to the same DCE solution (v/v = 1:1) containing Fc (5.0 mM), **Ru** (0.5 mM), and Bn-Br (50 mM) (Entry 2, Table 2). The partition coefficients (C_{H2O}/C_{DCE}; C_X indicates the concentration in phase X) of each compound were estimated to 2×10^{-5} (Fc), 8×10^{-4} (**Ru**), and 1×10^{-6} (Bn-Br), respectively, based on the absorption spectra of each solution phase of their biphasic solution. Hence, most of the compounds were initially distributed in the DCE phase. After visible-light irradiation (λ > 400 nm) for 1 h while stirring, the colorless aqueous phase turned blue, and the UV-vis absorption spectrum of the aqueous phase exhibited a characteristic absorption band centered at λ_{max} = 620 nm that was assigned to Fc^+ (Fig. 3b). In contrast, Fc^+ was not detected in the absorption spectrum of the DCE phase after photoirradiation (Fig. 3c), indicating that Fc^+, generated by the photooxidation of Fc by **Ru*** in the DCE phase, was completely transferred to the aqueous phase. In addition, Bn_2 was produced in the DCE phase after photolysis (Fig. S5c and d). The amount of produced Bn_2 (0.90 μmol) was roughly equivalent to half of the amount of Fc^+ (1.87 μmol) produced in the aqueous phase (Entry 2, Table 2), which satisfies the redox reaction shown in Eq. 4.

$$Fc + Bn\text{-}Br \xrightarrow{h\nu,\ PS} Fc^+ + 1/2Bn_2 + Br^- \quad (4)$$

In order to determine the role of each component in this photoreaction, control experiments were conducted. In the absence of light, **Ru**, or Fc, neither Fc^+ nor Bn_2 was produced, indicating that photoexcitation of **Ru** and the subsequent reduction by Fc are essential for the photocatalytic reaction (Entries 3–5, Table 2). Although Fc^+ was generated even in the absence of Bn-Br, the amount formed was extremely low because **Ru** cannot catalytically act as the redox photosensitizer in the absence of an electron acceptor such as Bn-Br (Entry 6, Table 2). Based on these results, we would like to propose a feasible mechanism for the photocatalytic reductive coupling of Bn-Br in H_2O/DCE biphasic solution (Scheme 2). The **Ru** photosensitizer is excited by irradiation with visible light (λ > 400 nm), followed by the reduction of **Ru*** with Fc, which takes place in the DCE phase. Subsequently, the generated one-electron-reduced species **Ru**$^-$ supplies an electron to Bn-Br, which produces Bn_2, whereas Fc^+ migrates from the DCE phase to the aqueous phase to accomplish the overall reaction.

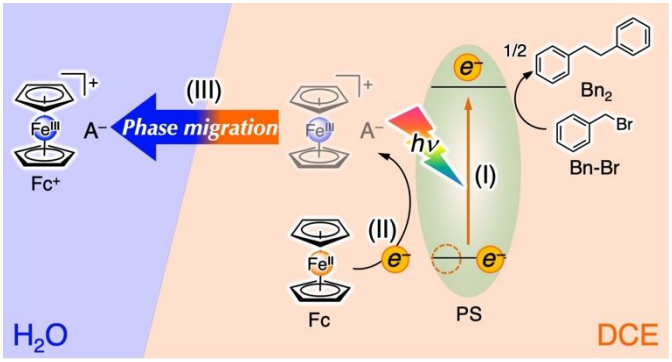

Scheme 2 Proposed mechanism for the biphasic photocatalysis of the reductive coupling of Bn-Br

The use of **Ir** instead of **Ru** promotes the biphasic photocatalysis more efficiently, *i.e.*, with a more than ten times higher turnover number (TON) for the generation of Bn_2 (Entries 2 and 7-9, Table 2). Especially when the concentration of the photosensitizer was decreased to 1/10 (0.05 mM), the TON remained unchanged or decreased only slightly when using **Ru** (Entries 2 and 7, Table 2), while it further increased by 6.7 times when using **Ir** (Entries 8 and 9, Table 2). As described above, **Ir** exhibits *ca.* eight times higher absorption (ε = 119,000 M^{-1} cm^{-1}) than **Ru** (ε = 15,000 M^{-1} cm^{-1}), which enables the absorption of >90% of incoming photons even at a concentration of **Ir** of 0.05 mM. Therefore, an improved TON was obtained when using a diluted solution of **Ir** (0.05 mM) as the photosensitizer. The higher absorbance of **Ir** can also be expected to reduce the absorption inhibition by coexisting Fc, which is commensurate with an inner-filter effect. Furthermore, the K_{SV} for the reductive quenching is more than sixty times higher for **Ir** (1.1×10^5 M^{-1}) than that for **Ru** (1.8×10^3 M^{-1}) due to the largely extended lifetime of the excited **Ir** compared to that of **Ru**

(Table 1). The high K_{SV} of **Ir** enables sufficient photoinduced electron transfer even if the concentration of Fc decreases with progressing reaction. The better absorption and longer excited lifetime of **Ir** should lead to enhanced photocatalytic activity.

It should also be noted here that the photoreduction of Bn-Br does not occur in DCE as a single-phase solution system, even when using **Ir** as the photosensitizer (Entry 10, Table 2). This fact strongly suggests that the phase migration of Fc^+ across a biphasic solution suppresses the unfavorable backward charge recombination, which enables the photoreduction of Bn-Br. To confirm this hypothesis, we examined the coexistence effect of Fc^+ in the biphasic photocatalysis. When Fc^+A^- (A^- = Cl^- or PF_6^-; 1.5 μmol) was initially added to a H_2O/DCE biphasic solution containing Bn-Br (50 mM), **Ir** (0.05 mM), and Fc (5 mM), the partition coefficients C_{H2O}/C_{DCE} of Fc^+A^- were determined to be 10.1 and 1.7 for A^- = Cl^- and PF_6^-, respectively (Fig. S6). Exposing these solutions to visible-light irradiation (λ > 400 nm) afforded different amounts of Bn_2, depending on the counter anion. Remarkably, the generation of Bn_2 was negligible in the presence of $Fc^+PF_6^-$ (green plots in Fig. 4). This inhibition indicates an accelerated charge recombination by Fc^+, which unequivocally resides in the DCE phase. On the other hand, the addition of Fc^+Cl^-, which resides predominantly in the aqueous phase, significantly suppresses the decrease in photocatalytic activity (blue *vs.* black plots in Fig. 4). Based on these results, we can conclude that Fc^+ species distributed in the DCE phase are more susceptible to engage in backward charge recombination with $\mathbf{Ir}^-$, and accordingly, phase migration of Fc^+ to the aqueous phase plays an important role for efficient photocatalysis. In fact, the addition of $NBu_4^+Br^-$, which accelerates phase migration, substantially improves the photocatalytic activity (*vide infra*; red plots in Fig. 4).

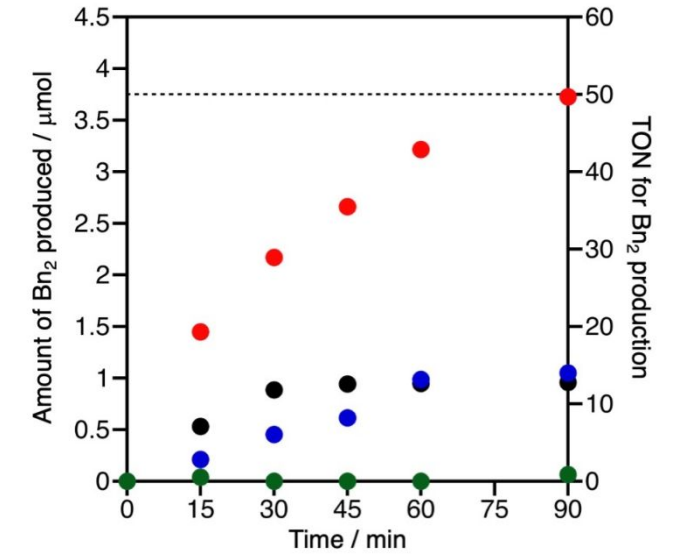

Fig. 4 Time course of the photochemical formation of Bn_2 in a H_2O/DCE (1:1, *v*/*v*) biphasic solution containing Bn-Br (50 mM), **Ir** (0.05 mM), and Fc (5 mM) without additives (black plots), in the presence of $Fc^+PF_6^-$ (1 mM, green plots), Fc^+Cl^- (1 mM, blue plots), or $NBu_4^+Br^-$ (5 mM, red plots) under irradiation with visible light (λ > 400 nm). The dashed line shows the upper limit of Bn_2 evolution expected from the amount of Fc added to these solutions.

Designing a biphasic solution to boost the coupled phase migration/photoinduced electron transfer to increase the efficiency of the photocatalysis

The aforementioned results on the coupled phase migration/photoinduced electron transfer prompted us to further investigate design principles in order to improve the efficiency of this photocatalytic reaction. Short diffusion distances, fast diffusion of the mediators to reach the liquid-liquid interface, and large interface areas should all accelerate the phase migration of the mediators.[35, 50-53] We found that the photoreduction of Bn-Br did not proceed when using **Ir** (0.05 mM) in the H_2O/DCE (1:1) biphasic solution without stirring (Entry 11, Table 2). On the other hand, the rate of photocatalytic Bn_2 formation increased upon increasing the H_2O/DCE ratio (Fig. 5a). Higher H_2O/DCE ratios can be expected to decrease the volume of the DCE droplets[51] and thus increase the opportunity for Fc^+ generated in DCE to reach the liquid-liquid interface with a shorter diffusion distance.[35, 50-53] These results suggest that the phase migration of Fc^+ is the rate-determining step in this biphasic reaction.

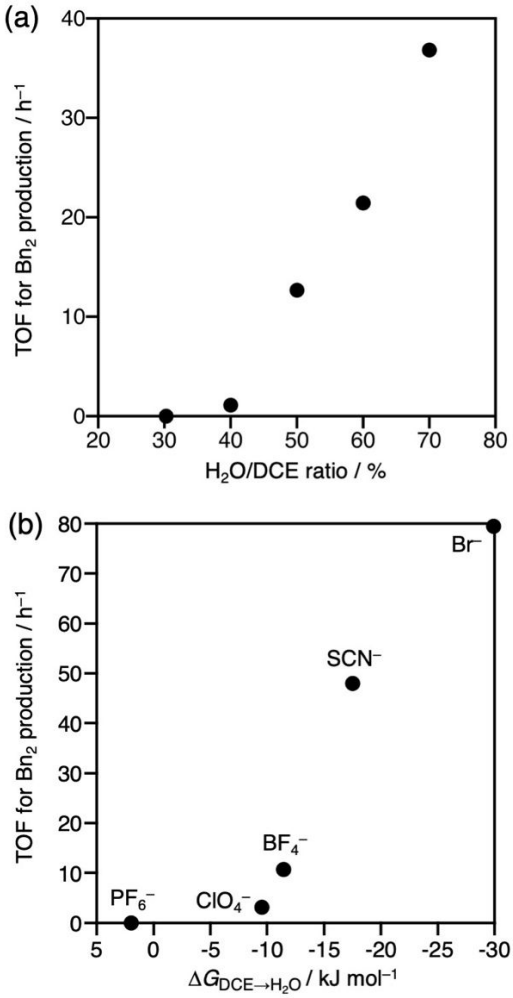

Fig. 5 Dependence of the TOF of the photoreduction of Bn-Br to afford Bn_2 on the (a) H_2O/DCE ratio and (b) Gibbs free energy of Fc^+A^- for the phase migration from DCE to H_2O ($\Delta G(Fc^+A^-)_{DCE\rightarrow H2O}$) in the presence of A^- (A^- = PF_6^-, ClO_4^-, BF_4^-, SCN^-, I^-, or Br^-). The biphasic H_2O/DCE solutions, which contain **Ir** (0.05 mM), Fc (5 mM), and Bn-Br (50 mM), were exposed to irradiation from visible light (λ > 400 nm).

Finally, the effects of coexisting ions on the biphasic photocatalysis were examined in order to chemically accelerate the phase migration of Fc^+. For the H_2O/DCE system, the Gibbs energy for ion migration of Fc^+ from the DCE phase to the aqueous phase ($\Delta G(Fc^+)_{DCE\rightarrow H2O}$) was reported to be –2.0 kJ mol^{-1}.[34] Photochemcally generated Fc^+ should cross the liquid-liquid interface accompanying an anion A^- to maintain the charge balance in solution. Hence, the Gibbs energies for the migration of the ion pair Fc^+A^- ($\Delta G(Fc^+A^-)_{DCE\rightarrow H2O}$) can be tuned by the Gibbs energy for phase migration of added anion ($\Delta G(A^-)_{DCE\rightarrow H2O}$) on the basis of Eq. 5.[54]

$$\Delta G(Fc^+A^-)_{DCE\rightarrow H2O} = \Delta G(Fc^+)_{DCE\rightarrow H2O} + \Delta G(A^-)_{DCE\rightarrow H2O} \quad (5)$$

A biphasic solution consisting of water (1.5 mL) and a DCE solution (1.5 mL) containing Fc (5.0 mM), **Ir** (0.05 mM), Bn-Br (50 mM), and $NBu_4^+A^-$ (5.0 mM; $A^- = PF_6^-$, ClO_4^-, BF_4^-, SCN^-, I^-, or Br^-) was irradiated ($\lambda > 400$ nm) for 1 h with stirring. The rates of photocatalytic Bn_2 formation were proportional to $\Delta G(Fc^+A^-)_{DCE\rightarrow H2O}$, which depends on the hydrophilicity of the anion used (Fig. 5b). A smaller $\Delta G(Fc^+A^-)_{DCE\rightarrow H2O}$ is commensurate with a distribution that leans more toward the aqueous phase in the presence of A^-. Increased photocatalytic activity was observed in the case of adding $NBu_4^+A^-$ with $A^- = SCN^-$ and Br^- while with $A^- = BF_4^-$, ClO_4^-, and PF_6^- decrease the activity relative to the case without adding $NBu_4^+A^-$ (TOF = 12.7 h^{-1}). Note that a control reaction between $NBu_4^+A^-$ ($A^- = Br^-$ or SCN^-) with relatively nucleophilic anions and Bn-Br without photosensitizer did not directly generate Bn_2, meaning that the role of added $NBu_4^+A^-$ is to modulate the photocatalytic processes shown in Scheme 2. It is also noteworthy that Fc^+ was detected predominantly in the aqueous phase after the photocatalytic reaction, regardless of the kind of salt added. However, once Fc^+A^- migrates to the aqueous phase, it may still kinetically return to the DCE phase during the photocatalytic reaction on account of the distribution equilibrium. Therefore, we can conclude that the use of anions with small $\Delta G(A^-)_{DCE\rightarrow H2O}$ values further decreases the backward charge recombination in DCE, thus increasing the efficiency of the photocatalytic formation of Bn_2. Furthermore, the TON of Bn_2 formation reached 50 (3.75 μmol), which is consistent with the complete consumption of the Fc electron donor (7.50 μmol), after continuous photocatalysis for 1.5 h in the presence of $NBu_4^+Br^-$ (red plots in Fig. 4). This result clearly indicates that photoinduced phase migration has a potential to overcome the backward charge recombination caused by Fc^+ generated during the photocatalysis.

The best photocatalytic performance for Bn_2 formation was recorded by adding $NBu_4^+Br^-$ (TOF = 79.5 h^{-1}; external quantum efficiency: 0.2%; λ = 480 nm). These values are comparable to those using sacrificial electron donors such as a trialkylamine,[55] an NADH derivative,[56] or a benzoimidazole derivative[57] in a single-phase organic solution (Table S1). These sacrificial electron donors usually irreversibly supply an electron to a photosensitizer due to fast deprotonation followed by irreversible dimerization, which suppresses backward charge recombination.[14, 15, 55, 57-60] However, the use of a sacrificial reductant should be avoided from a practical perspective because this strategy generates chemical waste and consumes energy.[15] In stark contrast, electron donors with sufficient redox durability may be able to act as redox mediators in the artificial Z-scheme photocatalysis,[37] providing access to useful "non-sacrificial" reactions such as water splitting,[16] CO_2 reduction,[15] and the reductive conversion of organic compounds[61] using, *e.g.*, water as an electron source.

Conclusions

In this study, we have developed a biphasic solution system that facilitates the photocatalytic reductive coupling of Bn-Br using Ru(II)- or Ir(III)-based photosensitizers and ferrocene (Fc) as an electron donor. We discovered that the phase migration of the photogenerated ferrocenium cation (Fc^+) plays an important role for the spatial charge separation and thus suppresses the backward charge recombination, which results in the successful photocatalytic reductive coupling of Bn-Br with an efficiency that is comparable to or better than that of reactions that use a sacrificial electron donor. Since photoinduced electron transfer to Fc^+ has already been reported,[62-64] the Fc^+ generated in the aqueous phase has the potential to be used as an electron acceptor for oxidative photocatalysis, *e.g.*, water oxidation, while recovering Fc in the organic phase. Therefore, the present study provides a new opportunity to construct unique and efficient Z-scheme photocatalysis systems where the phase-migratable Fc^+/Fc connects useful oxidation and reduction reactions separately driven in biphasic solutions.

Experimental

General procedures

$RuCl_3{\cdot}nH_2O$ (>99.9%), KPF_6 (>97.0%), NH_4PF_6 (>95.0%), and ferrocene (Fc; >98.0%) were purchased from Wako Pure Chemical Industries, Ltd. Ethylene glycol, $IrCl_3{\cdot}3H_2O$ (>90.0%), methanol (>99.8%), 2-ethoxyethanol (>98.0%), dichloromethane (>99.5%), 1,2-dichloroethane (DCE; >99.5%), acetonitrile (>99.9%), and *n*-hexane (>96.0%) were purchased from Kanto Chemical Co., Inc. $MgSO_4$ (>99.0%) and 4,4'-dimethyl-2,2'-bipyridine (dmb; >99.0%) were purchased from Sigma Aldrich. Coumarin 6 (C6; >98.0%), dibenzyl (Bn_2; >99.0%), $NBu_4^+PF_6^-$ (>98.0%), $NBu_4^+ClO_4^-$ (>98.0%), $NBu_4^+BF_4^-$ (>98.0%), $NBu_4^+SCN^-$ (>95.0%), $NBu_4^+I^-$ (>98.0%), and $NBu_4^+Br^-$ (>99.0%) were purchased from Tokyo Chemical Industry Co., Ltd. $Fc^+PF_6^-$ (>98.0%) was purchased from Santa Cruz Biology, Inc. Benzyl bromide (Bn-Br; >97.0%) was purchased from Nacalai Tesque, Inc. All these chemicals were used as received.

^1H NMR (500 MHz) spectra were measured on a JEOL ECZ-500R spectrometer. UV-vis absorption and emission spectra were recorded at room temperature on Shimadzu U1900i and Horiba FluoroMax-4 spectrophotometers, respectively. Emission lifetimes were measured on a Horiba DeltaFlex (excitation source: NanoLED-440L).

Elemental analyses were carried out on a PerkinElmer 2400 II CHN analyzer. Constituent elements were analyzed by electron dispersion X-ray spectroscopy on a Shimadzu EDX-7000 spectrometer. Cyclic voltammetry measurements were

conducted on a BAS model 650A electrochemical analyzer, using a glassy carbon working electrode and a platinum-wire counter electrode. The reference electrode was made of a silver wire, inserted into a small glass tube fitted with a porous Vycor frit at the tip, and filled with a CH_3CN solution containing 0.1 M $NBu_4^+PF_6^-$ and 0.01 M $AgNO_3$.

Synthesis

$[Ru(dmb)_3](PF_6)_2$ (**Ru**) was synthesized from $RuCl_3{\cdot}nH_2O$ and dmb according to a literature procedure.[47] ^{1}H NMR (500 MHz, acetone-d_6, Fig. S7a): δ 8.68 (s, 6H, 3,3'-Ar-H), δ 7.84 (d, J = 5.5 Hz, 6H, 6,6'-Ar-H), δ 7.38 (d, J = 4.5 Hz, 6H, 5,5'-Ar-H), δ 2.56 (s, 18H, CH_3). Calcd. for $C_{36}H_{36}N_6P_2F_{12}Ru$: C, 45.81; H, 3.85; N, 8.91; Found: C, 45.41; H, 3.96; N, 8.69.

$[Ir(C6)_2(dmb)]PF_6$ (**Ir**) was synthesized according to a slightly modified literature procedure.[46] An Ir(III) μ-chloro-bridged dimer complex, which was used as a precursor for the target complex **Ir** was synthesized as previously reported.[65] A suspension of the dimer complex (0.104 g, 0.056 mmol) and dmb (0.023 g, 0.125 mmol) in ethylene glycol (5.6 mL) was stirred for 2 h at 150 ºC under a nitrogen atmosphere. After cooling to room temperature, the reaction mixture was poured into water (40 mL) and NH_4PF_6 (0.407 g, 2.497 mmol in 4 mL of water) was added. The resulting precipitate was extracted into CH_2Cl_2 (2 × 50 mL), before the organic phase was separated, dried over $MgSO_4$, and filtered. After all volatiles had been removed from the filtrate under reduced pressure, the obtained crude product was purified by column chromatography on silica gel (methanol/CH_2Cl_2 = 5:95, v/v), followed by recrystallization from CH_2Cl_2/n-hexane, which afforded **Ir** as red crystals (0.086 g, 0.068 mmol, 63% yield). ^{1}H NMR (500 MHz, acetone-d_6, Fig. S7b): δ 8.85 (d, J = 6.0 Hz, 2H), δ 8.53 (s, 2H), δ 8.08 (d, J = 8.5 Hz, 2H), δ 7.77 (d, J = 5.0 Hz, 2H), δ 7.31 (t, J = 7.2 Hz, 2H), δ 7.02 (t, J = 7.2 Hz, 2H), δ 6.42 (d, J = 3.5 Hz, 2H), δ 6.17 (d, J = 9.5 Hz, 2H), δ 6.10-6.07 (m, 4H), δ 3.40 (q, J = 7.7 Hz, 6H), δ 2.60 (s, 6H), δ 1.06 (t, J = 7.3 Hz, 12H). Anal. Calcd. for $C_{52}H_{46}F_6IrN_6O_4PS_2{\cdot}0.5CH_2Cl_2$: C, 49.91; H, 3.75; N, 6.65. Found: C, 49.80; H, 3.67; N, 6.59.

Ferrocenium chloride (Fc^+Cl^-) was synthesized by treating an aqueous $Fc^+PF_6^-$ solution for 60 min with an Amberlite IRA-900J ion-exchange resin (Cl form) at room temperature under nitrogen sparging to avoid decomposition by O_2,[66-68] followed by removal of the solvent under reduced pressure. The anion exchange from PF_6^- to Cl^- was confirmed by electron dispersion X-ray spectroscopy (Fig. S8). UV-vis absorption: λ_{max} = 618 nm.

Emission-quenching measurements

DCE solutions of the **Ru** (0.006 mM) and **Ir** (0.00025 mM) were prepared in the absence or presence of Fc at various concentrations (0-0.3 mM) or Bn-Br at various concentrations (0-3.0 mM). Each solution was placed into a quartz cell and purged with nitrogen gas for 20 min. Assuming conditions that satisfy the Stern-Volmer relationship described in Eq. 2, Stern-Volmer constants (K_{SV}) and quenching rate constants (k_q) were determined by plotting the relative emission intensity (I_0/I) as a function of the concentration of the quencher Fc.

Photocatalytic reactions

A solution of Fc (5.0 mM), photosensitizer (0.5 or 0.05 mM), and Bn-Br (50 mM) in DCE (1.5 mL) was placed in a test tube (inner diameter: 10 mm; volume: 8.4 mL), before water was added (0.65-3.50 mL). The partition coefficient of each component was estimated based on the absorption spectra in each solution phase before photoirradiation. Note that the molar extinction coefficients were assumed to be the same in DCE and water for Fc and Bn-Br, because they are hardly dissolved in water. The photographs of the reaction solution were shown in Fig. S9. The biphasic solution was degassed by nitrogen sparging (10 min) and irradiated using a 300 W Xe lamp (Cermax) through a cutoff filter (L-42; λ > 400 nm). Unless otherwise noted, stirring was continued during photoirradiation. The products of the aqueous phase, *i.e.*, Fc^+ was analyzed by UV-vis absorption spectra in a quartz cell (1 mm × 10 mm; ε = 308 M^{-1} cm^{-1} at 620 nm), while the DCE phase, *i.e.*, Bn_2, was analyzed by high performance liquid chromatography. HPLC analyses were performed on a Shimadzu LC-20AT system equipped with a Phenomenex column (250 × 4.6 mm, 4 mm). A CH_3CN/H_2O (80:20, v/v) solution was used as the eluent at a flow rate of 1.0 mL min^{-1} (column temperature: 313 K), and a Shimadzu CBM-20A diode array was used as the detector. Under these analytical conditions, the retention times were determined using purchased or as-prepared samples (Bn-Br: 4.2 min; Fc: 6.2 min; Bn_2: 7.2 min) (Fig. S10). A LED lamp (CL-H1-470-9-1, Asahi Spectra Co.) combined with a 480 nm (fwhm = 10 nm) band-pass filter (Asahi Spectra Co.) was used instead of the Xe lamp to irradiate with monochromatic light (480 nm) in order to determine the quantum efficiency (Φ) for the formation of Bn_2 according to Eq. 6:

$$\Phi = \frac{\text{Amount of Bn}_2\text{ produced (mol)}}{\text{Inputted photon (einstein)}} \quad (6)$$

Conflicts of interest

There are no conflicts to declare.

Acknowledgements

This work was supported by a Grant-in-Aid for Scientific Research on Innovative Areas "Innovation for Light-Energy Conversion (I^4LEC)" from MEXT (JP20H05113 and JP20H05093). The authors also acknowledged for the financial supports from JSPS KAKENHI grants JP19K23652 and JP19H02736, by a MEXT KAKENHI grants JP18H05517 (Hydrogenomics), by the JST PRESTO grant JPMJPR20T5 (Controlled Reaction), and by the Research Promotion Fund from the Promotion and Mutual Aid Corporation for Private Schools of Japan.

References

1. A. Thilagam, *J. Math. Chem.*, 2014, **53**, 466-494.
2. Y. Wang, H. Suzuki, J. Xie, O. Tomita, D. J. Martin, M. Higashi, D. Kong, R. Abe and J. Tang, *Chem. Rev.*, 2018, **118**, 5201-5241.

3. W. J. Ong, L. L. Tan, Y. H. Ng, S. T. Yong and S. P. Chai, *Chem. Rev.*, 2016, **116**, 7159-7329.
4. Y. Yamazaki, H. Takeda and O. Ishitani, *J. Photochem. Photobiol. C*, 2015, **25**, 106-137.
5. X. Liu, S. Inagaki and J. Gong, *Angew. Chem., Int. Ed.*, 2016, **55**, 14924-14950.
6. L. Zou, R. Sa, H. Lv, H. Zhong and R. Wang, *ChemSusChem*, 2020, **13**, 6124-6140.
7. H. Wang, X. Meng, G. Zhao and S. Zhang, *Green Chem.*, 2017, **19**, 1462-1489.
8. B. K. Banik, B. Banerjee, G. Kaur, S. Saroch and R. Kumar, *Molecules*, 2020, **25**, 5918-5941.
9. J. H.Alstrum-Acevedo, M. K. Brennaman and T. J. Meyer, *Inorg. Chem.*, 2005, **44**, 6802-6827.
10. D. Gust, T. A. Moore and A. L. Moore, *Acc. Chem. Res.*, 2009, **42**, 1890-1898.
11. A. Iwase, Y. H. Ng, Y. Ishiguro, A. Kudo and R. Amal, *J. Am. Chem. Soc.*, 2011, **133**, 11054-11057.
12. Y. Tachibana, L. Vayssieres and J. R. Durrant, *Nat. Photonics*, 2012, **6**, 511-518.
13. S. Fukuzumi, K. Ohkubo and T. Suenobu, *Acc. Chem. Res.*, 2014, **47**, 1455-1464.
14. A. Nakada, K. Koike, T. Nakashima, T. Morimoto and O. Ishitani, *Inorg. Chem.*, 2015, **54**, 1800-1807.
15. Y. Tamaki, K. Koike, T. Morimoto and O. Ishitani, *J. Catal.*, 2013, **304**, 22-28.
16. R. Abe, K. Sayama and H. Sugihara, *J. Phys. Chem. B*, 2005, **109**, 16052-16061.
17. A. Nakada, H. Suzuki, V. Jhon Junie Magdadaro, K. Ogawa, M. Higashi, A. Saeki, A. Yamakata, H. Kageyama and R. Abe, *ACS Appl. Mater. Inter.*, 2019, **11**, 45606-45611.
18. Y. Sasaki, H. Kato and A. Kudo, *J. Am. Chem. Soc.*, 2013, **135**, 5441-5449.
19. D. G. Nocera, *Acc. Chem. Res.*, 2012, **45**, 767-776.
20. N. Nelson and A. Ben-Shem, *Nat. Rev. Mol. Cell. Biol.*, 2004, **5**, 971-982.
21. S. Eberhard, G. Finazzi and F. A. Wollman, *Annu. Rev. Genet.*, 2008, **42**, 463-515.
22. D. Gust, T. A. Moore and A. L. Moore, *Acc. Chem. Res.*, 2001, **34**, 40-48.
23. S. Berardi, S. Drouet, L. Francàs, C. Gimbert-Suriñach, M. Guttentag, C. Richmond, T. Stoll and A. Llobet, *Chem. Soc. Rev.*, 2014, **43**, 7501-7519.
24. J. R. Bacon and C. M. Davidson, *Analyst*, 2008, **133**, 25-46.
25. A. Leo, C. Hansch and D. Elkins, *Chem. Rev.*, 1971, **71**, 525-616.
26. K. Fent, A. A. Weston and D. Caminada, *Aquat. Toxicol.*, 2006, **76**, 122-159.
27. B. Nowack and T. D. Bucheli, *Environ. Pollut.*, 2007, **150**, 5-22.
28. S. Liu, Q. Li and Y. Shao, *Chem. Soc. Rev.*, 2011, **40**, 2236-2253.
29. M. Paidar, V. Fateev and K. Bouzek, *Electrochim. Acta*, 2016, **209**, 737-756.
30. L. Zong and C. H. Tan, *Acc. Chem. Res.*, 2017, **50**, 842-856.
31. K. B. Oldham, *J. Solid State Chem.*, 1998, **2**, 367-377.
32. H. Moon and J. H. Park, *Anal. Chem.*, 2021, **93**, 16915-16921.
33. C. K. Terry Weatherly, M. W. Glasscott and J. E. Dick, *Langmuir*, 2020, **36**, 8231-8239.
34. J. Hanzlik, Z. Samec and J. Hovorka, *J. Electroanal. Chem.*, 1987, **216**, 303-308.
35. P. Tasakorn, J. Chen and K. Aoki, *J. Electroanal. Chem.*, 2002, **533**, 119-126.
36. K. Aoki, P. Tasakorn and J. Chen, *J. Electroanal. Chem.*, 2003, **542**, 51-60.
37. C. K. Terry Weatherly, H. Ren, M. A. Edwards, L. Wang and H. S. White, *J. Am. Chem. Soc.*, 2019, **141**, 18091-18098.
38. E. Vladimirova, P. Peljo and H. H. Girault, *J. Electroanal. Chem.*, 2018, **816**, 242-252.
39. H. N. Kagalwala, D. N. Chirdon, I. N. Mills, N. Budwal and S. Bernhard, *Inorg. Chem.*, 2017, **56**, 10162-10171.
40. S. Rastgar and G. Wittstock, *J. Phys. Chem. C*, 2017, **121**, 25941-25948.
41. Y. H. Hong, Y. M. Lee, W. Nam and S. Fukuzumi, *J. Am. Chem. Soc.*, 2022, **144**, 695-700.
42. Y. Zhang, J. L. Petersen and C. Milsmann, *Organometallics*, 2018, **37**, 4488-4499.
43. H. Yin, P. J. Carroll, J. M. Anna and E. J. Schelter, *J. Am. Chem. Soc.*, 2015, **137**, 9234-9237.
44. G. Park, S. Y. Yi, J. Jung, E. J. Cho and Y. You, *Chemistry*, 2016, **22**, 17790-17799.
45. B. H. Farnum, A. Nakada, O. Ishitani and T. J. Meyer, *J. Phys. Chem. C*, 2015, **119**, 25180-25187.
46. S. Y. Takizawa, N. Ikuta, F. Zeng, S. Komaru, S. Sebata and S. Murata, *Inorg. Chem.*, 2016, **55**, 8723-8735.
47. A. Ito, N. Kobayashi and Y. Teki, *Inorg. Chem.*, 2017, **56**, 3794-3808.
48. E. Schott, X. Zarate and R. Arratia-Perez, *J. Phys. Chem. A*, 2012, **116**, 7436-7442.
49. A. Einstein, *Ann. Phys.*, 1905, **322**, 549-560.
50. I. Benjamin, *Science*, 1993, **261**, 1588-1560.
51. K. Nakatani, M. Sudo and N. Kitamura, *J. Phys. Chem. B*, 1998, **102**, 2908-2913.
52. C. E. Banks, T. J. Davies, R. G. Evans, G. Hignett, A. J. Wain, N. S. Lawrence, J. D. Wadhawan, F. Marken and R. G. Compton, *Phys. Chem. Chem. Phys.*, 2003, **5**, 4053-4069.
53. S. Park, D. H. Han, J. G. Lee and T. D. Chung, *ACS Appl. Energy Mater.*, 2020, **3**, 5285-5292.
54. H. Katano, K. Uematsu, Y. Kuroda and T. Osakai, *Anal. Sci.*, 2019, **35**, 1031-1035.
55. J.-M. Kern and J.-P. Sauvage, *J. Chem. Soc., Chem. Commun.*, 1987, 546-548.
56. K. Hironaka, S. Fukuzumi and T. Tanaka, *J. Chem. Soc. Perkin Trans. 2*, 1984, 1705-1709.
57. Y. Zhang, J. L. Petersen and C. Milsmann, *J. Am. Chem. Soc.*, 2016, **138**, 13115-13118.
58. A. Nakada, K. Koike, K. Maeda and O. Ishitani, *Green Chem.*, 2016, **18**, 139-143.
59. Y. Tamaki and O. Ishitani, *ACS Catal.*, 2017, **7**, 3394-3409.
60. Y. Yamazaki, A. Umemoto and O. Ishitani, *Inorg. Chem.*, 2016, **55**, 11110-11124.
61. C. K. Prier, D. A. Rankic and D. W. C. MacMillan, *Chem. Rev.*, 2013, **113**, 5322-5363.
62. X.-B. Xia, Z.-F. Ding and J.-Z. Liu, *J. Photochem. Photobiol. A*, 1995, **88**, 81-84.
63. S. Fery-Forgues and B. Delavaux-Nicot, *J. Photochem. Photobiol. A*, 2000, **132**, 137-159.
64. M. E. B. Santiago, C. Declet-Flores, A. Díaz, M. M. Vélez, M. Z. Bosques, Y. Sanakis and J. L. Colón, *Langmuir*, 2007, **23**, 7810-7817.
65. S. Sebata, S. Y. Takizawa, N. Ikuta and S. Murata, *Dalton Trans.*, 2019, **48**, 14914-14925.

66. A. Singh, D. R. Chowdhury and A. Paul, *Analyst*, 2014, **139**, 5747-5754.
67. J. P. Hurvois and C. Moinet, *J. Organomet. Chem.*, 2005, **690**, 1829-1839.
68. G. Zotti, G. Schiavon, S. Zecchin and D. Favretto, *J. Electroanal. Chem.*, 1998, **456**, 217-221.